AD-A269 120

ADVANCED OPTICAL FIBER COMMUNICATION SYSTEMS

Professor Leonid G. Kazovsky, Principal Investigator

Department of Electrical Engineering

Durand 202, MC-4055

Stanford University

Stanford, CA 94305-4055

DTIC
ELECTE
SEP 10 1993
S **D**
A

ABSTRACT

Our research is focused on three major aspects of advanced optical fiber communication systems: dynamic wavelength division multiplexing (WDM) networks, high dynamic range coherent analog optical links, and fiber nonlinearities. In the area of WDM networks, a prototype high-speed interface board between workstation and WDM network has been designed, implemented, and tested, with a highest data rate so far of 728 Mbps. We also began the theoretical investigation of a system using combined ASK/DPSK modulation formats. The results show the feasibility of using semiconductor lasers with ASK/DPSK combined modulation in future dynamic WDM network. In the area of high dynamic range coherent analog optical links, we completed analyses of the spurious-free dynamic range (SFDR) of coherent amplitude and coherent angle modulated links and compared the results with those for conventional and optically preamplified direct detection links. In the area of fiber nonlinearities, we showed that the pdf of four wave mixing interference is non-Gaussian and analyzed the impact of four wave mixing on the attainable receiver sensitivity of coherent WDM digital systems for both dispersion-shifted and non-dispersion-shifted fiber.

A more detailed summary of our research is contained in the following sections.

93-20917

93 9 08 101

1. WDM Networks

High Speed Computer Interface of STARNET: STARNET is an optical broadband local area network based on a physical passive star topology intended for backbone applications. Over a single physical network, STARNET offers all users both a moderate-speed packet switched subnetwork and a reconfigurable high-speed (up to 2.5 Gbps) Wavelength Division Multiplexed (WDM) circuit switched subnetwork. Based on these two data transport facilities, several topological and protocol solutions are available to the users. As a result, STARNET supports traffic of widely different speed and continuity characteristics .The STARNET network serves high performance workstations running distributed multimedia applications, including video-conferencing. The moderate-speed interface uses an off-the-shelf FDDI-on-copper module to interface to the STARNET optics; a custom high-speed interface module provides fast packet switching (electronic) over the circuit switched (wavelength) subnetwork. In this report an ongoing effort aimed at the realization of the electronic hardware which interfaces the workstation to the STARNET optics is described.
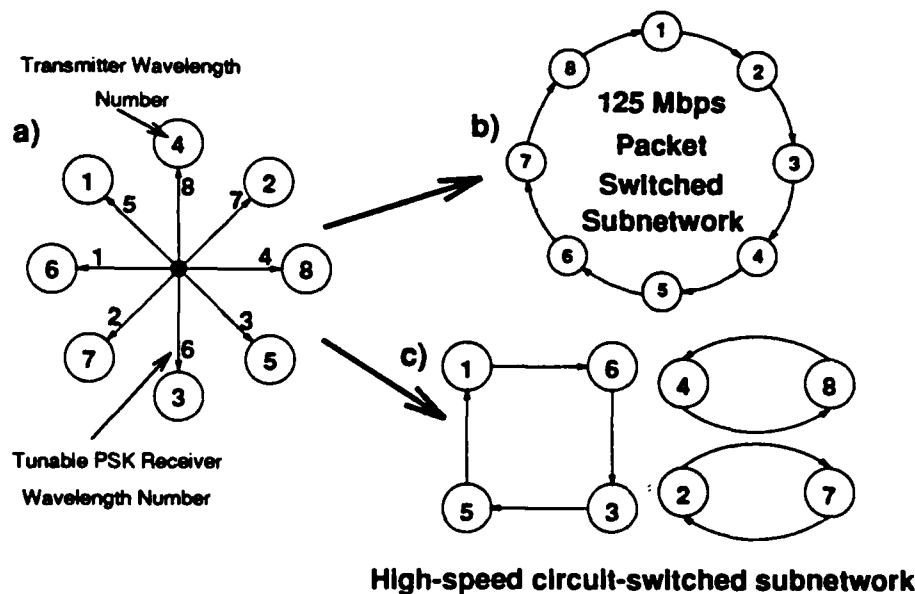
Fig. 1. Through the use of WDM, STARNET maps a physical star topology, a), into both, b), a logical ring topology in the moderate-speed subnetwork, and, c), reconfigurable, variable size rings in the high-speed subnetwork.

Fig. 1 shows how STARNET, through the combination of WDM and coherent optical reception, permits two simultaneous and independent logical subnetworks over a single physical passive star. The moderate-speed subnetwork is configured by tuning each node's

2

coherent heterodyne ASK receiver to the previous node's transmitter wavelength forming a fixed logical ring topology. The reconfigurable high-speed subnetwork nodes use their wavelength-tunable coherent heterodyne PSK receiver to form several high-speed connections (point-to-point or ring). Each high-speed sub-group is independent and communication on the subrings is simultaneous. Sub-groups can come or go or change size as deemed necessary by the network traffic under control of reconfiguration software. The communication required to set up virtual circuits and to configure the high-speed subnetwork is done over the moderate-speed subnetwork.

It is important to note that the high-speed subnetwork is considered to be circuit-switched because the lasers used in the wavelength tunable receivers tune very slowly, on the order of seconds. Therefore, the various sub-rings that make up the high-speed subnetwork are relatively long lasting (compared to most connections such as file transfers, e-mail, etc. However, in order to provide both topological flexibility and higher network throughput, it is necessary to provide electronic packet-switching at each node. In other words, the high-speed subnetwork topology is circuit-switched, while the data over the high-speed subnetwork is packet-switched.
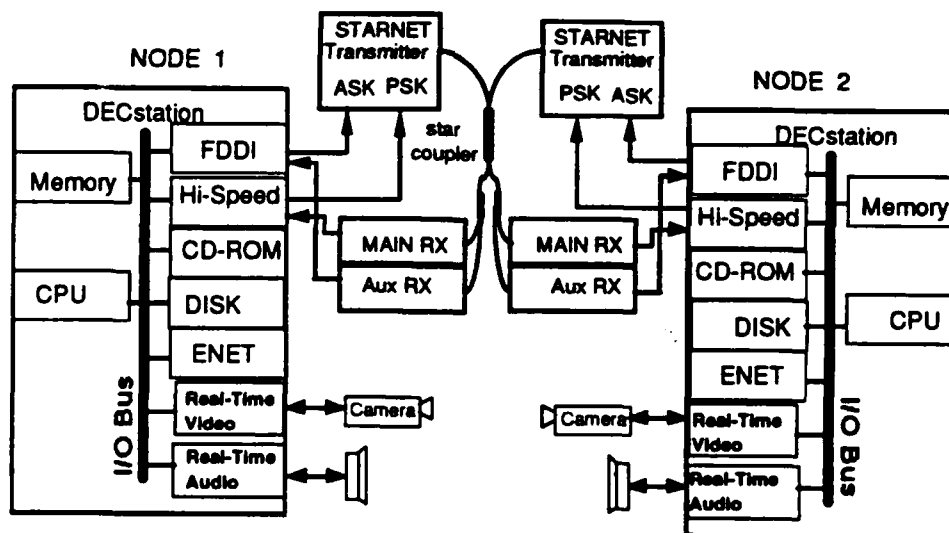

Fig. 2. Two node experiment.

A schematic of an experimental two node STARNET interconnecting two DECstation 5000/240 workstations is shown in Fig. 2. Each workstation is equipped with built-in Ethernet and SCSI ports. Off-the-shelf TURBOchannel bus interface cards provide real-time video and

3

real-time audio. Access to a CD-ROM is provided over the SCSI port. We will run an assortment of multimedia applications over STARNET.

In addition, two TURBOchannel cards are used to interface to the STARNET transceivers. An off-the-shelf FDDI-on-copper board connects via coax directly to the STARNET transceiver's ASK port. We have successfully formed a four-node FDDI ring using STARNET optics to form one leg of the ring. The FDDI ring thus formed is strictly conventional and required no modifications to either the hardware or the software. Over this subnetwork we will setup a control channel which will be used to setup, configure and monitor status of the high-speed subnetwork. A custom designed TURBOchannel interface card provides the workstation access to the high-speed PSK links provided by the STARNET transceiver.
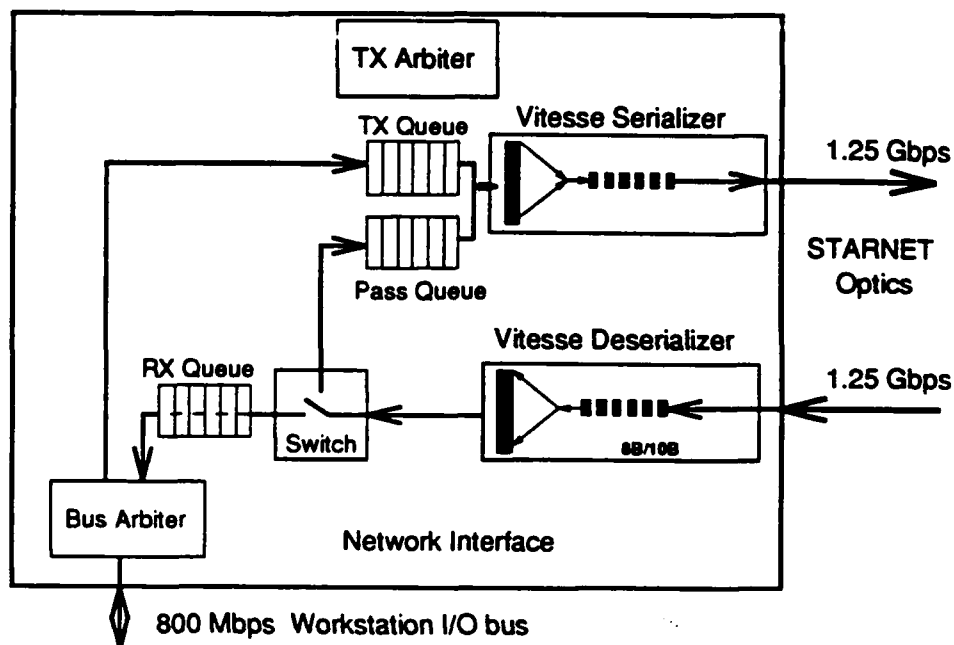

Fig. 3. Block diagram of the high-speed subnetwork interface board.

A simplified block diagram of the high-speed subnetwork interface is shown in Fig.3. The main elements are three FIFO queues, the TURBOchannel bus arbiter, an arbiter for transmitting packets over the high speed link, and a routing switch for received packets. The TURBOchannel bus arbiter chip is implemented in an Altera 7256 Field Programmable Gate Array (FPGA) and includes full I/O and DMA access over the TURBOchannel. Functionality in the chip includes arbitration between transmit and receive requests. The transmit arbiter is implemented in an Altera 7032 FPGA and uses the same general scheme as the bus arbiter. The routing switch is

4

implemented in an Altera 7256 FPGA with an external Dual Port RAM which acts as a routing lookup table. The FIFOs provide for queuing of packets before they are switched to their final destination (either on to the network, into host memory or both).

A separate board from Vitesse provides (de)serialization of data words as well as 8B/10B encoding. Therefore, the serial line rate is 1.25 Gbps while the data rate is 1.0 Gbps The workstations' TURBOchannel I/O bus, however, provides half-duplex data transfer at a burst rate of 800 Mbps. Furthermore, the bus I/O bandwidth must be shared with other devices on the bus (e.g. FDDI packet subnetwork, Ethernet, SCSI, etc.).A liberal estimate of the I/O bandwidth available to the high-speed subnetwork that can be sustained is 300 Mbps full-duplex. Therefore, the STARNET transceiver is capable of sending/receiving at a rate several times greater than that which the TURBOchannel can sustain, which creates a one of the `bottlenecks' in the interface.
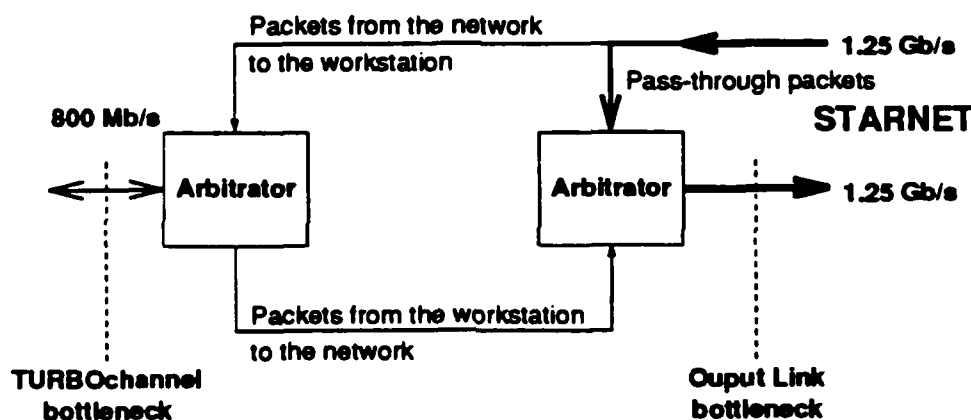

Fig. 4. Bottlenecks in the high-speed network interface.

There are, in fact, two bottlenecks associated with the high-speed network interface: the TURBOchannel and the 1.0 Gbps output link. The TURBOchannel bandwidth must be shared between the workstation's input and output data streams; the output link must be shared between the workstation's output stream and pass-through traffic. The allocation of bandwidth at each bottleneck is done in hardware by two arbitrators, as shown in Fig.4. The arbitrators operate as follows: a two-slot cycle is formed, and each of the time slots is allocated to one of the competing streams. By adjusting the time slot sizes, it is possible to control the amount of

bandwidth allocated to each stream; this adjustment can be done by software. The process is illustrated in Fig.5. The granularity in the time slot sizes is one packet, and if one stream is idle, then the whole bandwidth is available to the other stream.

A wide variety of traffic will coexist simultaneously on the high-speed network. This traffic will include file transfers, e-mail, videoconferencing, etc. These services have different bandwidths and tolerance to packet loss. For example, file transfer can be high or low bandwidth and must be delivered error free. Therefore, file transfer is high-priority from a packet loss point of view. Real-time services such as videoconferencing are typically high bandwidth and tolerate packet loss within a given quality of service target. We have conducted experiments to measure the maximum transmission and reception performance of the high-speed interface. The performance is variable and depends upon host memory loading, but on average is 643 Mbps (out of the 800 Mbps theoretical maximum). The interface board could support 728 Mbps but was reduced by excess latency introduced the workstation.

1)

TX	PASS
T	T

2)

TX	PASS
T_1	T_2
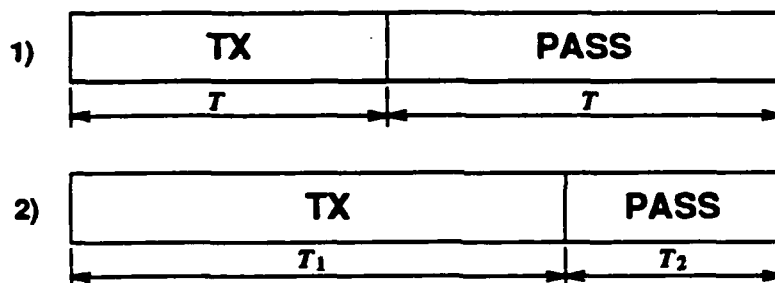
Transmit Bandwidth, TX, set point negotiated over control subnetwork.

Interface responds dynamically to burstiness by (de)increasing the short term bandwidth when the network is uncongested.

Interface remains fair when the network is congested by enforcing the long term bandwidth allocation (neither Pass nor Tx streams starve).

Fig. 5. Dynamic bandwidth allocation in the high-speed network interface.

To date, the high-speed interface board prototype has been completed. Debugging of the transmit and retransmit portions of the interface has been fully completed. Debugging of the receive portion is well underway and is now limited to only the addition of the ability to DMA packets directly into the application buffer rather than to an intermediate buffer in the Unix kernel. Upon completion of the debugging of the prototype, we will have PC boards constructed for up to four nodes.

Combined Modulation Formats for STARNET: STARNET (described previously) is a computer communications network which utilizes wavelength-division multiplexing (WDM) and coherent detection. The present STARNET experiment uses a combined modulation format consisting of 2.488 Gb/s phase shift keying (PSK) and 125 Mb/s amplitude shift keying (ASK). STARNET processes high-speed circuit-switched payload data with a synchronous PSK receiver and lower-speed packet-switched network control data with a nonsynchronous ASK receiver at each node. The advantage of combined modulation in STARNET is the potential for accommodation of circuit-switched and packet-switched traffic on a single physical star topology through the creation of multiple logical sub-networks. Combined ASK/PSK modulation creates a tradeoff between the attainable PSK and ASK receiver sensitivities. The ASK modulation depth has been optimized experimentally at Stanford to give an overall system sensitivity of -32 dBm.

The present STARNET experiment employs phase-locking in synchronous PSK receivers, and thus requires the use of low-linewidth lasers (such as Nd:YAGs) as transmitters and local oscillators. To use conventional semiconductor lasers as STARNET transmitters, we are investigating combined modulation formats which are more resistant to linewidth-induced degradation. One such format consists of differential PSK (DPSK) for circuit-switched data and ASK for packet-switched data. *System diagrams for both DPSK and ASK modulation are shown* in Fig. 6, parts (a) and (b), respectively. The DPSK receiver utilizes delay-and-multiply detection and does not require a phase-locked loop. The ASK receiver is the same as in the present STARNET implementation.

We analyzed the performance of the DPSK/ASK modulation format for the STARNET application. The models take into account laser phase noise, receiver noise (shot and thermal), and nonideal IF and lowpass filtering. The filters are modeled as finite integrators, and the impact of such filters on the phase and receiver noises is taken into account. Preliminary results are presented in Fig. 7. A photodiode responsivity of unity and negligible thermal noise are assumed for all plots. Realistic IF filter bandwidths of 7.5 GHz and 6.25 GHz are assumed in the DPSK and ASK receivers, respectively. The graphs show DPSK and ASK receiver sensitivities versus the ASK modulation depth.
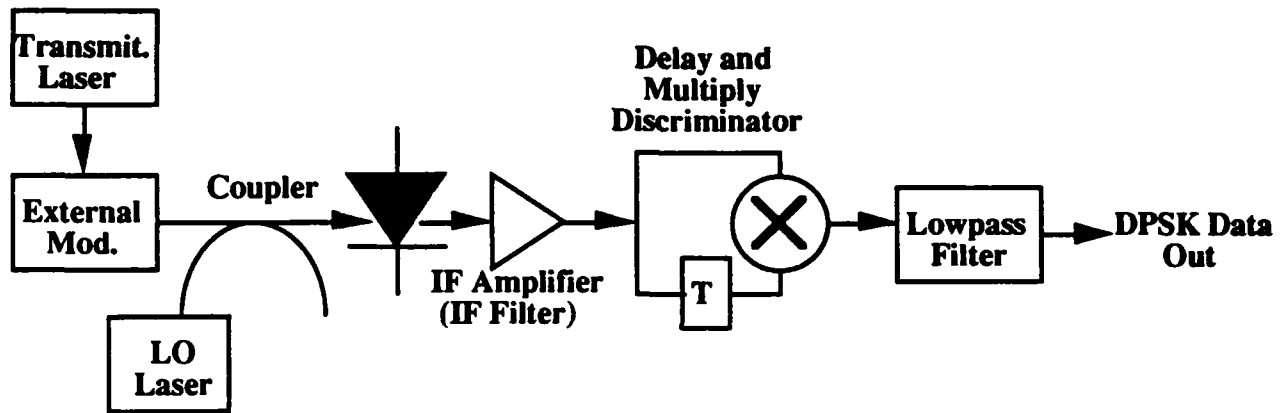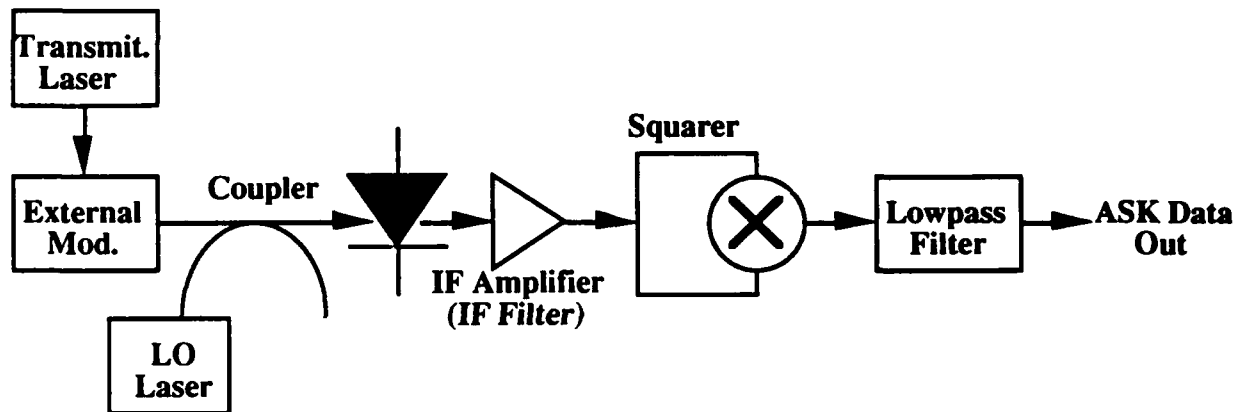
Fig. 6. Block diagrams of (a) DPSK heterodyne system with delay and multiply detection and (b) ASK heterodyne system using envelope detection.

Graph 7(a) assumes an ideal phase modulation depth of +/- 90 degrees. For this case, a combined linewidth of 1% of the DPSK bit rate (25 MHz) causes a performance degradation of approximately 3 dB. The optimum ASK modulation depth shifts from about 0.48 for zero linewidth to about 0.39 for a 25 MHz combined linewidth, since an increase in optical power is needed to compensate for the increase in linewidth, which causes degradation of DPSK receiver performance.
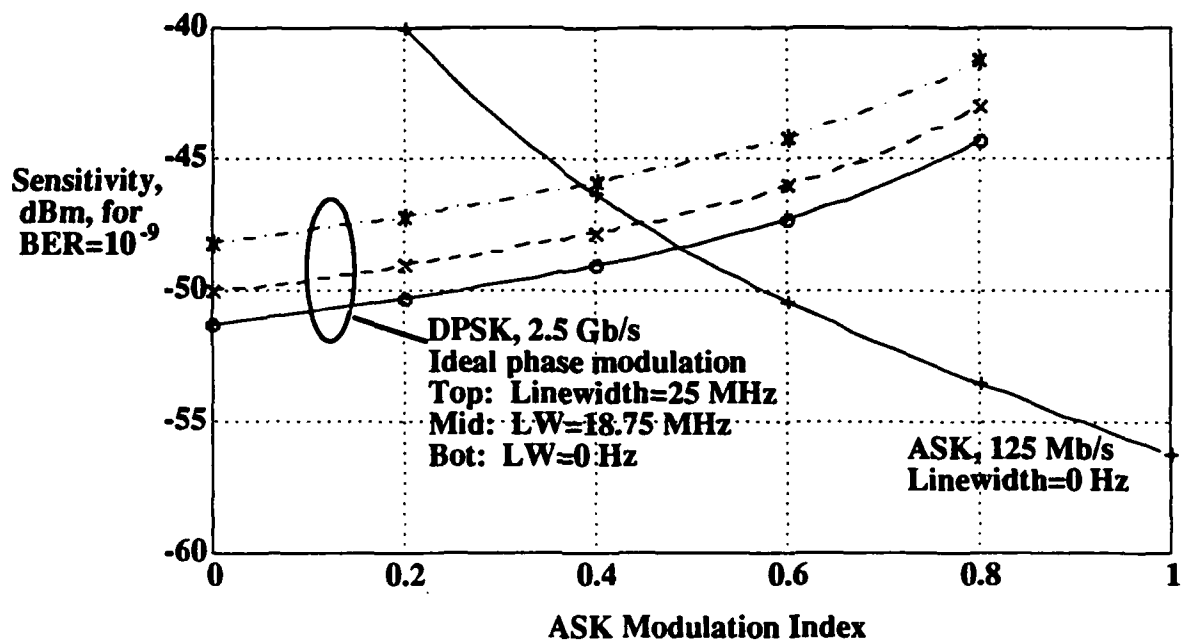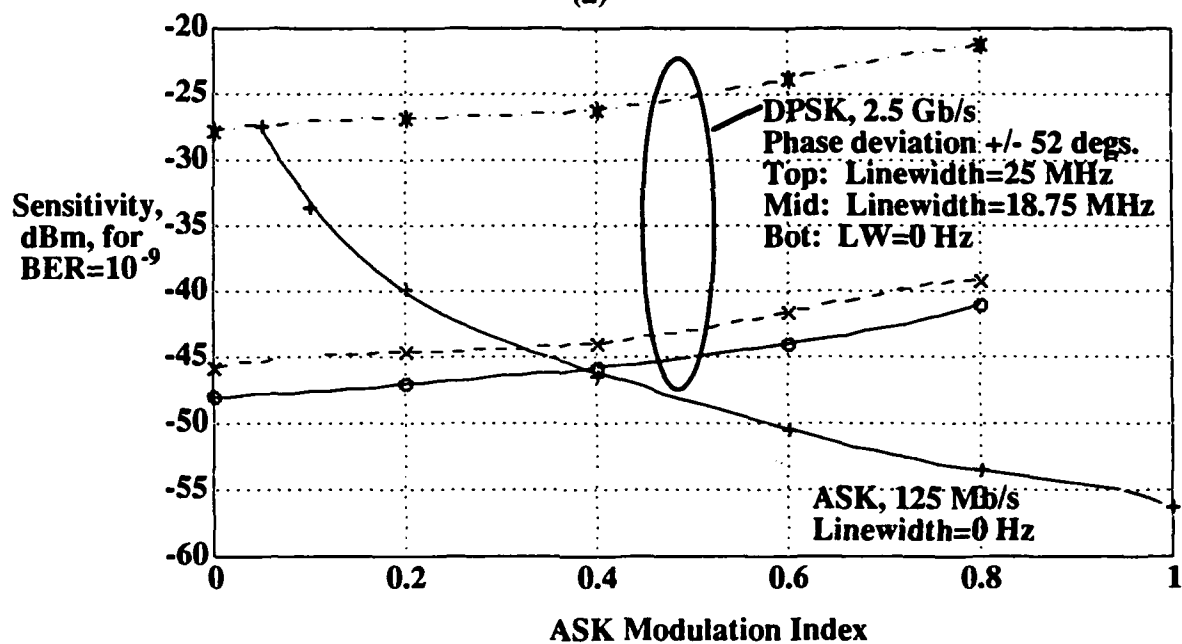
Fig. 7. Theoretical plots of DPSK and ASK receiver sensitivities versus ASK modulation depth for several values of laser linewidth. Plot (a) is for ideal phase modulation; plot (b) is for a phase deviation of +/- 52 degrees.

9

Graph (b) assumes a phase modulation depth of +/- 52 degrees, which is the maximum depth attainable in the present STARNET implementation; a greater modulation depth can be obtained with greater amplification of the electrical input. This results in a penalty, for zero linewidth, of about 3 dB for DPSK. For this case, a combined linewidth of 25 MHz (1% of the DPSK bit rate) causes a performance degradation of about 20 dB, which indicates that the bit error rate (BER) floor occurs at about 10^{-9}. Under these circumstances, the optimum ASK modulation depth is nearly zero, so that nearly all power is used for DPSK transmission.

These results indicate that the use of semiconductor lasers in future STARNET implementations is feasible, provided that the transmitter and local oscillator have sufficiently low linewidths to give acceptable receiver sensitivities. Since the linewidth-induced degradation of DPSK depends on the bit rate, each transmitter/local oscillator pair should be used with a DPSK bit rate at least 125 times the combined linewidth of the lasers. Also, the lasers should satisfy the power and tunability requirements dictated by the overall network configuration.

2. Coherent Analog Links

Optically preamplified direct-detection links: We theoretically investigated the performance of optically preamplified direct-detection links and compared their performance with that of coherent AM links analyzed in the previous report. A block diagram of an optically preamplified direct-detection link is shown in Fig. 8. The optical amplifier is used to boost the received optical signal before photodetection. As with any amplifiers, it adds noise to the signal that is amplified. As a result of the incoherent nature of spontaneous emission, spontaneous emission noise is added to the amplified signal. The polarization analyzer passes the desired signal and blocks the light in the orthogonal polarization. The optical filter is used to remove excess spontaneous emission noise. The noise power at the output of the electrical filter is:

$$N = \left\{ \eta_{th} + 2qRGP_s + R^2G^2P_s^2 10^{RIN/10} + 4R^2G(G-1)P_s n_{sp}h\nu + \left[R(G-1)n_{sp}h\nu \right]^2 (2B_o - B) \right\} B \quad (1)$$

where η_{th} is the thermal noise intensity, RIN is the relative intensity noise, n_{sp} (= 1) is the spontaneous emission factor, q is the electron charge, $h\nu$ is the photon energy, R (= 1.25 A/W) is the photodetector responsivity, G (= 15 dB) is the optical amplifier gain, P_s is the received optical power, B and B_o are the electrical and optical bandwidths, respectively. The first three terms in expr. (1) correspond to the thermal noise, shot noise and RIN while the last two terms originate

10

from the beating of spontaneous emission noise against itself and signal, respectively. Therefore, the spurious free dynamic range (SFDR) is

$$SFDR = 4\left(\frac{G^2 R^2 P_i^2}{N}\right)^{2/3} \tag{2}$$

RF input, x(t)

Transmitter laser

Fiber

Amplitude modulator

Optical Amplifier

Polarization Analyzer

Optical Filter
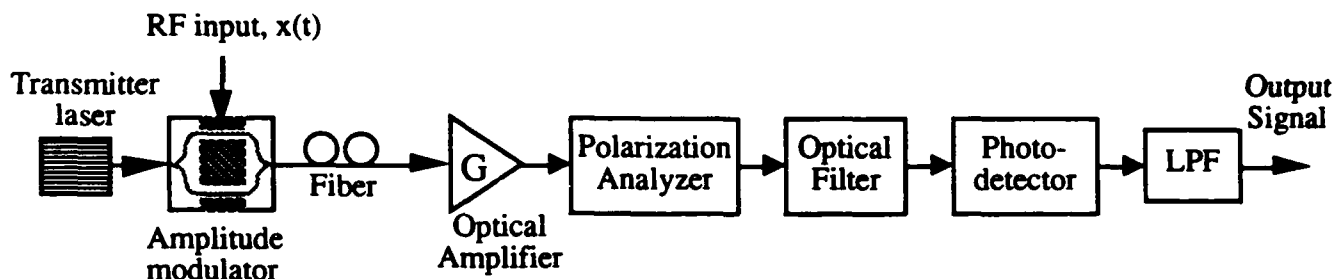
Photo-detector

LPF

Output Signal

Fig. 8. Block diagram for the optically preamplified direct detection link.

Fig. 9 shows the externally modulated coherent AM link studied in the previous report. It has been shown that preamplified direct-detection and heterodyne receiver have equivalent performance under shot noise-limited condition for digital systems. Here, we show that the same is true for shot noise-limited analog systems. However, for RIN-limited analog links, the preamplified links have a SFDR of about 4 dB higher than that of the coherent AM links.
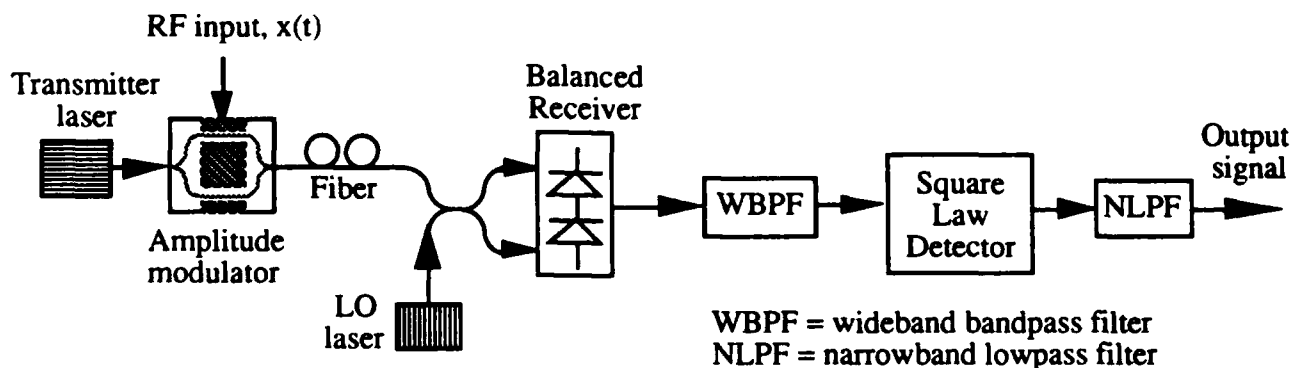
RF input, x(t)

Transmitter laser

Fiber

Amplitude modulator

Balanced Receiver

LO laser

WBPF

Square Law Detector

NLPF

Output signal

WBPF = wideband bandpass filter
NLPF = narrowband lowpass filter

Fig. 9. Block diagram for the coherent AM link.

In Fig. 10, the SFDR is plotted against the received optical power for the direct detection link (with and without an optical amplifier) and the coherent AM links. For small received

optical power (P_s < 1 mW), the preamplified link and the coherent link have very similar performance; they are both shot noise-limited (due to the optical gain for the preamplified link and due to the strong LO power for the coherent link). *The shot noise-limited SFDR for these two links is 107 dB·(Hz/mW)^{2/3} while it is 109 dB·(Hz/mW)^{2/3} for the conventional direct detection link.* For the preamplified link, the penalty is due to the 3 dB noise figure of the optical amplifier.
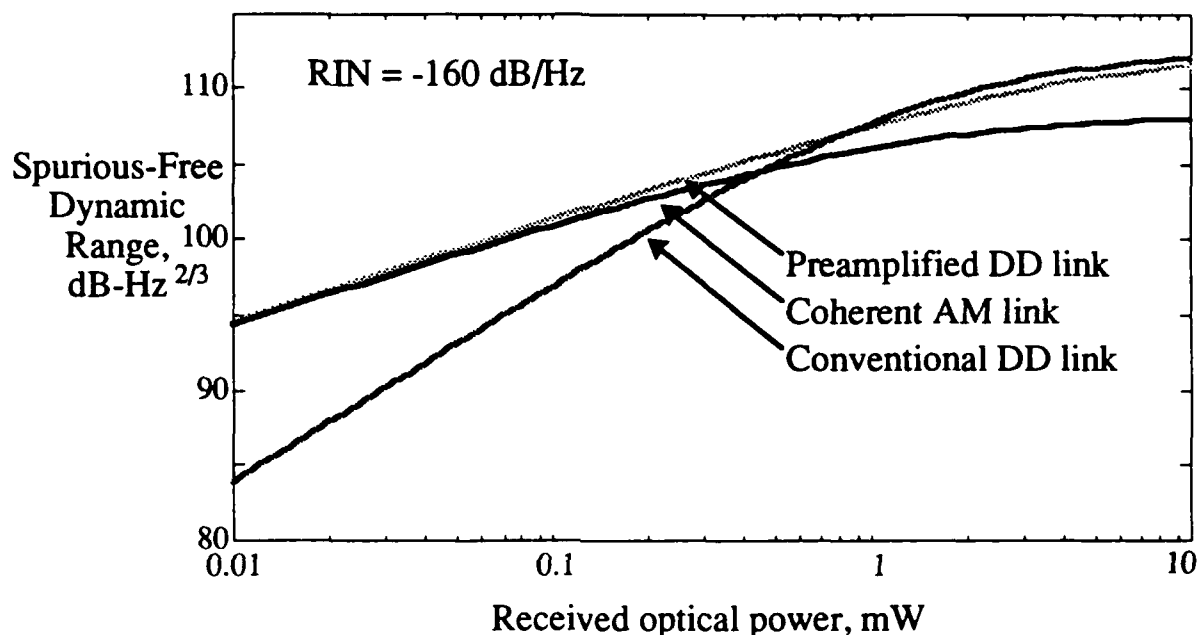

Fig. 10. Spurious-free dynamic range versus received optical power.

In Fig. 11, the SFDR is plotted against the laser RIN for the three links: the direct detection (with and without an optical amplifier) and the coherent AM links. When RIN starts to dominate (RIN > -140 dB/Hz), the penalty due to the noise figure of the optical amplifier decreases and the performance of the preamplified direct-detection link approaches that of the conventional direct detection link; so, the two links have the same RIN-limited performance. One can also see that the coherent AM link is more susceptible to RIN than the direct detection links. RIN starts to dominate at a low level (RIN > -150 dB/Hz) and it's RIN-limited SFDR is 4 dB less than that of the direct detection links.
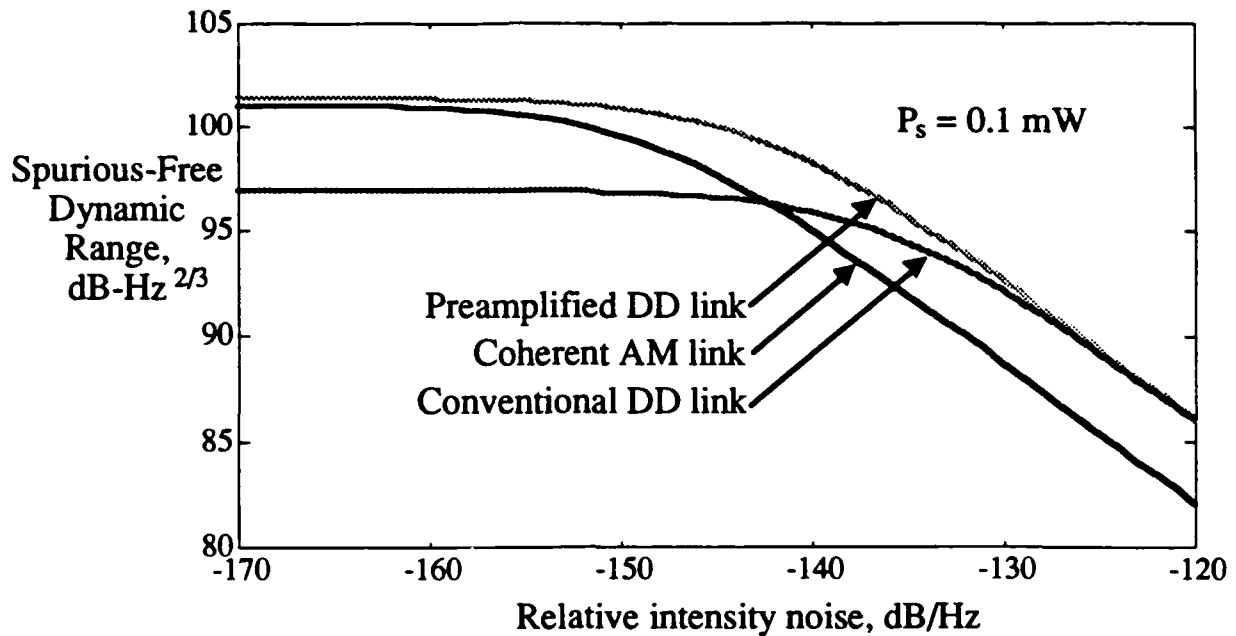
12

Fig. 11. Spurious-free dynamic range versus relative intensity noise.

To summarize, we have compared the performance of optically preamplified direct detection links with that of conventional direct detection and coherent AM links. Under shot noise limited condition, optically preamplified direct-detection links have same performance as coherent AM links. However, coherent AM links are more susceptible to RIN.

Our next step is to investigate the impact of adding an optical amplifier (with or without optical filter) to coherent AM links. We will compare the resulting performance with the other links we have studied.

Angle-Modulated Systems: In the previous report, we described the heterodyne interferometric phase modulated (HIPM) link, which improves the spurious free dynamic range (SFDR) over than of a direct detection (DD) link. The improvement is attained for two reasons. First, due to the inherent linearity of optical phase modulation, the SFDR of the HIPM link is limited by the nonlinearity of the microwave delay-line filter. This filter has a third-order intermodulation coefficient which is lower than that of the DD link. Second, the effect of laser relative intensity noise (RIN) on the HIPM link is suppressed to a greater extent than its effect on the DD link, as a result of the high intermediate frequency and the presence of a limiter in the receiver. In this report, we describe phase modulated (PM) and frequency modulated (FM) angle-modulated coherent links using external modulation. Both links have the same advantages as the HIPM link over the DD link. The difference is that the HIPM link is immune to phase noise effects. Due to the presence of a local oscillator laser before the photodiode, the effect of phase noise on coherent angle-modulated links will be significant if semiconductor distributed feedback (DFB) lasers are used. We present the results of a performance comparison between the coherent PM and FM links, the DD link, and the coherent AM link. The DD and AM links have been described in previous reports. We also evaluate the laser linewidth requirements for coherent PM and FM links to outperform the coherent AM link.
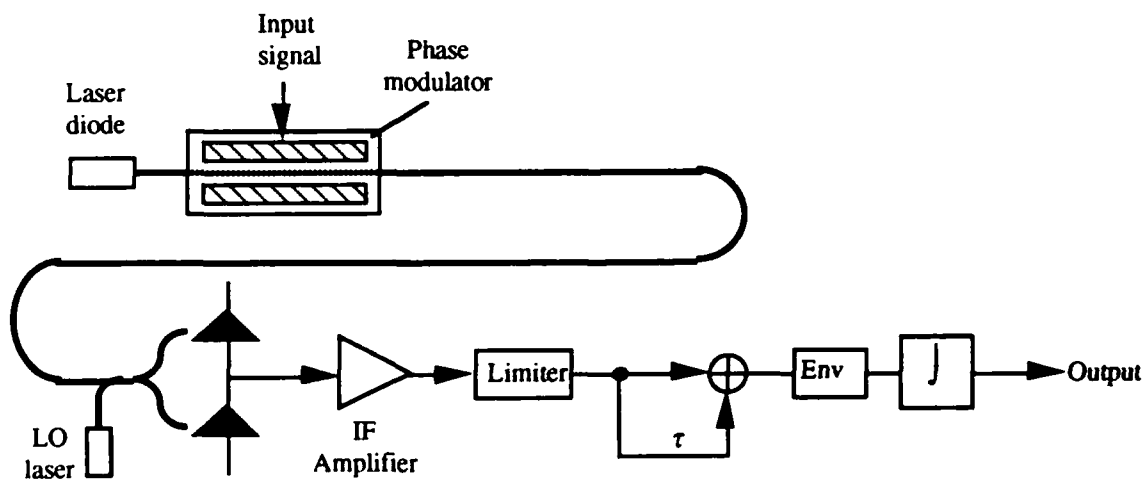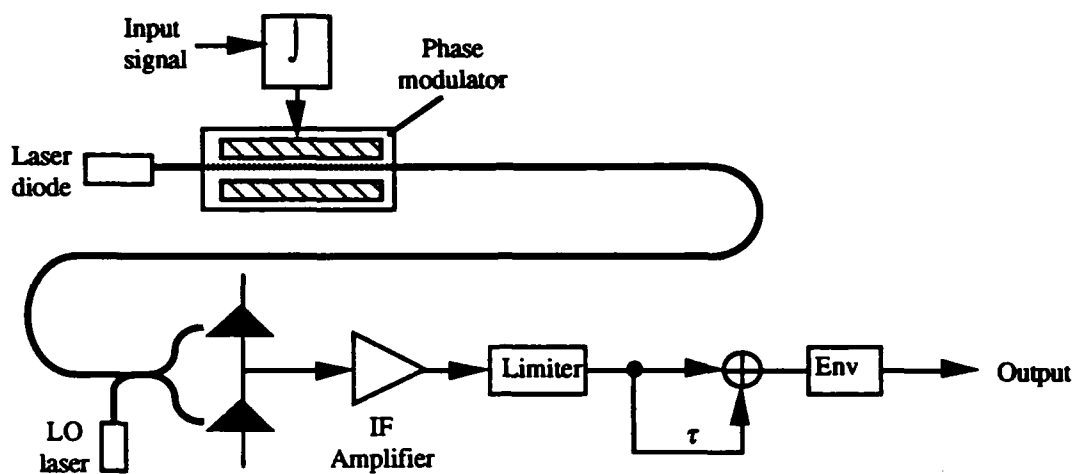

Fig. 12. (a) PM link

Fig. 12. (b) FM link

Fig. 12. Block diagrams of the PM and FM coherent links

The PM and FM coherent links are shown in Fig. 12. In the PM system, the input signal is phase-modulated on an optical carrier. At the receiver, the signal is combined with the LO laser light and detected. It is then amplified at the IF, limited, put through a delay line filter, envelope detected, and integrated. In the FM system, the input signal is integrated before being applied to a phase modulator. The FM receiver is identical to the PM receiver, except that there is no integrator before the output.

In Fig. 13, we evaluate the SFDR of the PM, FM, DD, and AM links. The transmitter and local oscillator are assumed to be DFB lasers with a linewidth of 10 MHz, a RIN power spectral density of -155 dB/Hz, and a RIN roll-off frequency of 3 GHz. At signal power levels less than 1 mW, the SFDR of the DD link is dominated by receiver thermal noise and its curve has a slope of 4/3. Above 1 mW, shot noise and RIN become significant. In the RIN-limited regime, the DD link SFDR is independent of signal power (slope of 0). At low signal levels, the coherent AM link SFDR is dominated by LO shot noise (slope of 2/3), and shows a marked advantage over the DD link. At higher power levels, the coherent AM link has an intrinsic disadvantage with respect to the DD link due to the extra baseband RIN and shot noise encountered in a heterodyne receiver.

At very low signal power levels (< -30 dBm), the SFDR of the PM and FM links is dominated by LO shot noise. However, above -30 dBm, phase noise is dominant and the SFDR is essentially independent of signal power level (slope of 0) for both the PM and FM links.
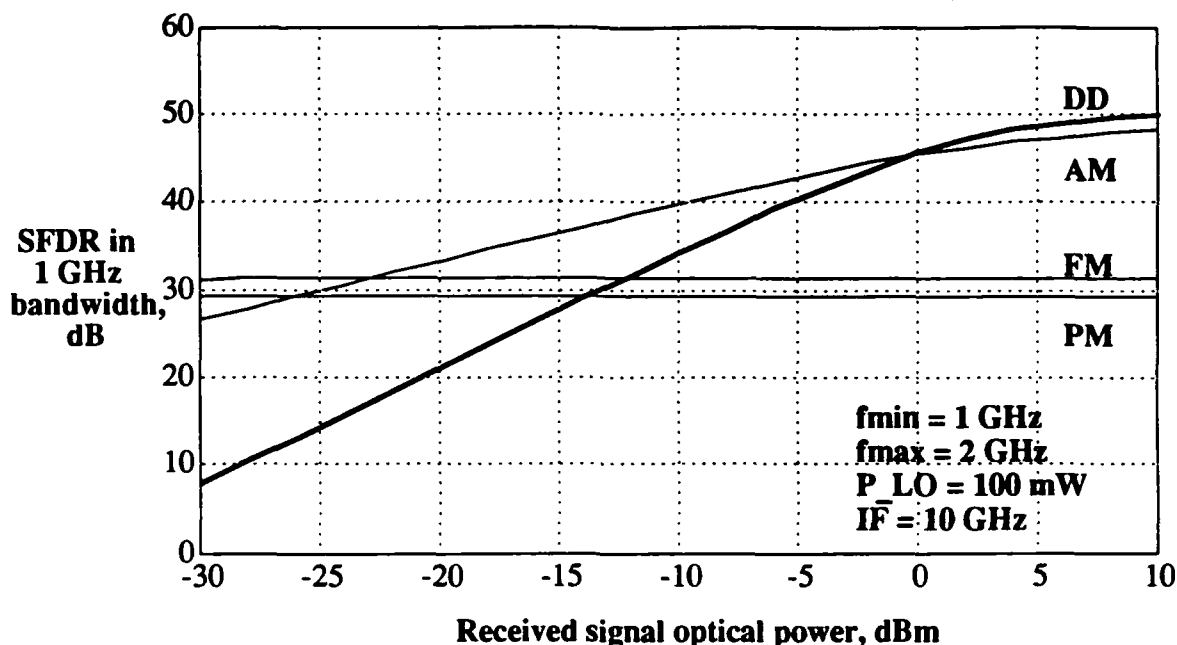
15

Fig. 13. SFDRs of DD, AM, PM, and FM links plotted against received signal optical power for a DFB laser with linewidth = 10 MHz and RIN = -155 dB/Hz.

Fig. 14 shows plots of SFDR vs. laser linewidth for the PM, FM, and AM links for received signal powers of -30 dBm, -15 dBm, and 0 dBm. The signal and local oscillator lasers are both assumed to have the same and constant linewidths at each point on the plot. As expected, the SFDR of the AM link is linewidth-independent. The SFDRs of the PM and FM links are strongly affected by linewidth. At low received power levels, the linewidth has little impact, since the receiver performance is dominated by thermal noise. At high received power levels, the impact of phase noise is severe, with the SFDR being reduced by 7 dB for every factor of 10 increase in the linewidth. At signal power levels of -30 dBm, -15 dBm, and 0 dBm, the phase noise becomes dominant over all other noises for linewidths of 5 MHz, 200 kHz, and 5 kHz, respectively. At signal power levels of -30 dBm, -15 dBm, and 0 dBm, the maximum allowable combined linewidths of the signal
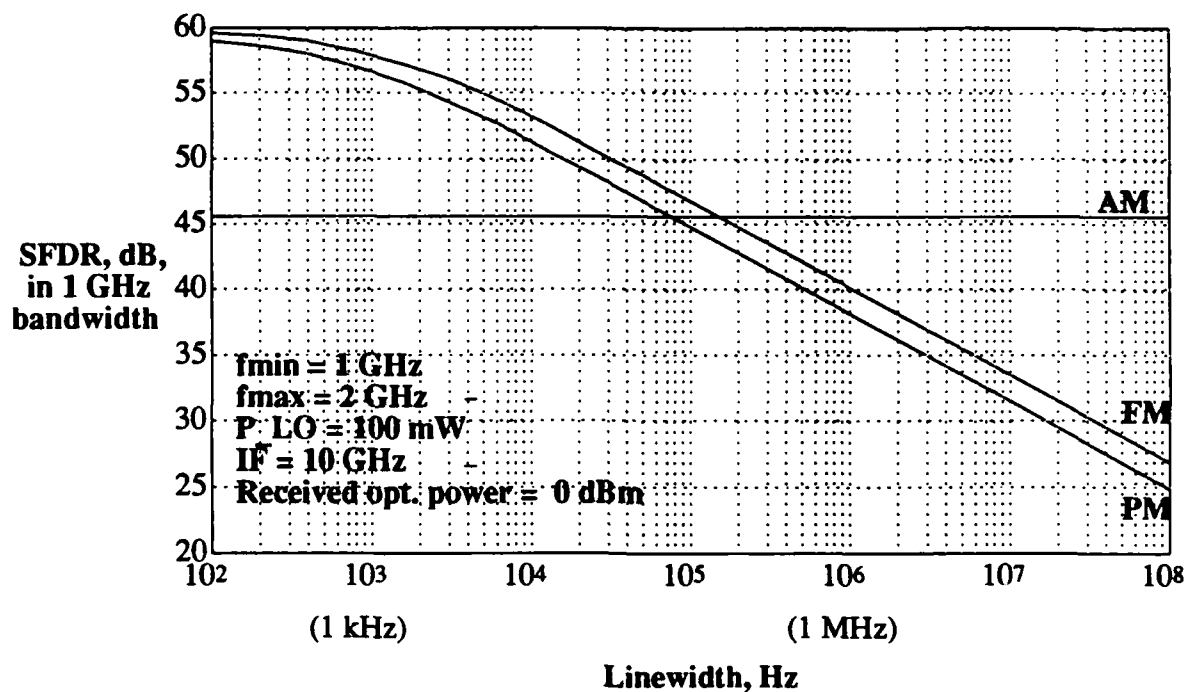
16

SFDR, dB, in 1 GHz bandwidth

fmin = 1 GHz
fmax = 2 GHz
P LO = 100 mW
IF = 10 GHz
Received opt. power = 0 dBm

AM

FM

PM

(1 kHz)

(1 MHz)

Linewidth, Hz

Fig. 14 (a)

SFDR, dB, in 1 GHz bandwidth

fmin = 1 GHz
fmax = 2 GHz
P LO = 100 mW
IF = 10 GHz
Received opt. power = -15 dBm

AM

FM

PM

(1 kHz)

(1 MHz)

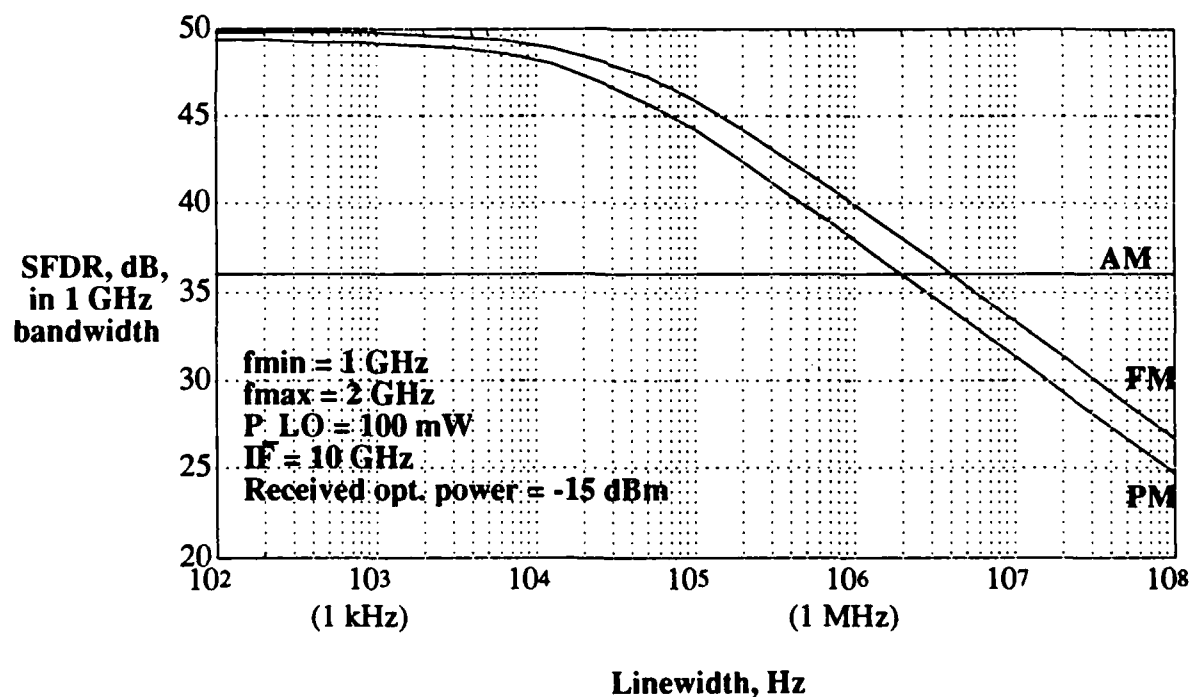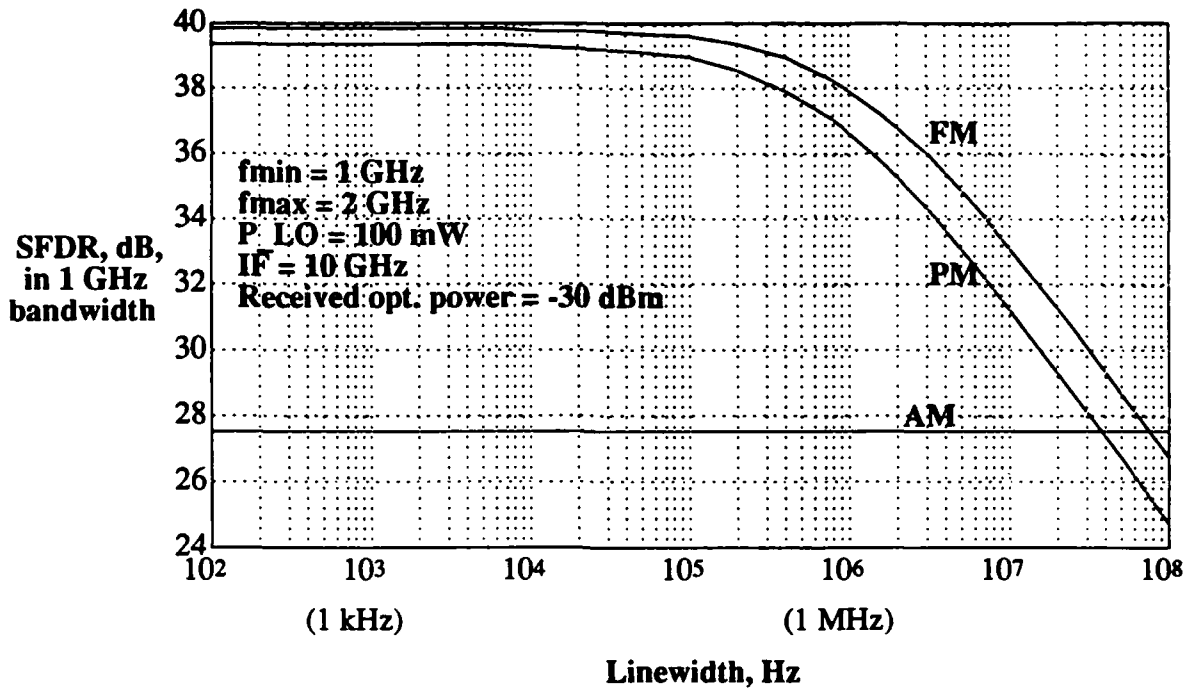**Linewidth, Hz**

Fig. 14 (b)

17

Fig. 14 (c)

Fig. 14. SFDRs of PM, FM, and AM links plotted versus linewidth for received signal power
levels of (a) 0 dBm; (b) -15 dBm; and (c) -30 dBm.

and LO lasers for the SFDRs of the PM and FM links to exceed that of the AM link are 70 kHz, 2 MHz, and 40 MHz, respectively. Thus, for optical powers under 1 mW, where the coherent AM link exhibits an SFDR advantage over the DD link, it is possible to gain SFDR improvements over the AM link by using the PM or FM links with lasers which have linewidths under 100 kHz.

3. Impact of Fiber Nonlinearities on Optical Communication Systems

Statistical Distribution of Four-Wave Mixing Interference in ASK Optical WDM Systems :The four-wave mixing (FWM) effect in optical fiber is caused by the third order nonlinear susceptibility of the fiber. If the frequency of the newly generated wave lies within the desired signal band, the resulting interference leads to crosstalk between channels and degrades system performance. In a wavelength-division-multiplexed (WDM) optical system, the number of interference terms increases rapidly with the number of channels. The power of each FWM interference term is proportional to the cube of the power of the incident waves, and increases with transmission distance. The combined effect of a large number of FWM interference terms is

18

treated as a Gaussian random process in some publications. However, the phase relationship between the interference terms makes the interference deviate from a Gaussian process. We performed computer simulations to investigate the statistical properties of the FWM interference. The simulation results are compared with the Gaussian approximation results.

Our simulation program simulates a coherent ASK (amplitude-shifted-keying) optical WDM system. In the program, several independent optical channels are computer-generated with random laser phase noise, uncorrelated random data streams, and independent clocks with random jitter. The program also generates all FWM interference terms that fall within the frequency band of the received channel. Each FWM term is calculated analytically. Next, the program evaluates the pdf of the sum of these FWM terms both at IF and at the envelope detector output.

The following numerical results are shown for the 8th channel (the worst case) of a 16-channel WDM system with a link of 100 km dispersion shifted fiber when all the channels except the 8th are transmitting '1'. The rest of system parameters are as follows: incident optical power = 0.1 mW/channel, wavelength = 1.55 μm, attenuation = 0.2 dB/km, channel spacing = 10 GHz, bit rate = 1 Gbit/s, laser linewidth = 10 MHz, A_{eff} = 55 μm^2, nonlinear susceptibility χ_{1111} = 6x10^{-15} cm^3/erg, responsivity = 0.6 amp/watt, and group velocity dispersion = 0.5 ps/km·nm.

Fig. 15 shows the simulated pdf's of the sum of the FWM interference terms at IF when the received channel is transmitting '0'. The in-phase component represents the component of the FWM interference that is in-phase with the desired signal at IF, and the quadrature-phase component represents the one that is 90 degrees out-of-phase with the IF. The main lobe of the simulated pdf is seen to match very well with the Student's t-distribution for both in-phase and quadrature-phase components. The corresponding Gaussian pdf is also shown in Fig. 15 for comparison. In expanded scale, we find that the tails of the simulated pdf's drop off slower than the Gaussian pdf, and tend to decay exponentially.

Fig. 16 shows the simulated pdf of the voltage at the envelope detector output for '0' transmission. A Gamma distribution is seen to match the simulated pdf very well. If the interference had a Gaussian-like behavior at the IF, the voltage at the envelope detector output should have a Rayleigh distribution. The corresponding Rayleigh distribution is also shown in Fig. 16 for comparison. It can be found by expanding the scale in Fig. 16 that the simulation results have larger tails than the Rayleigh distribution corresponding to the Gaussian approximation.
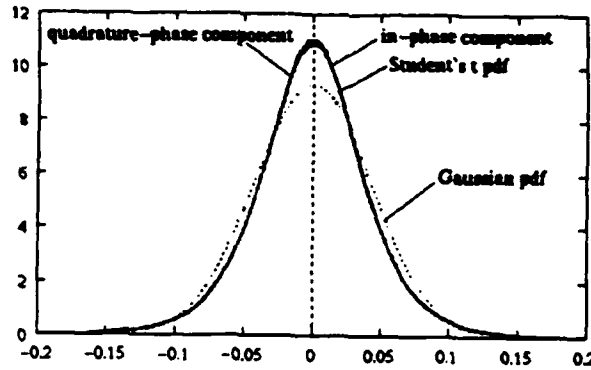
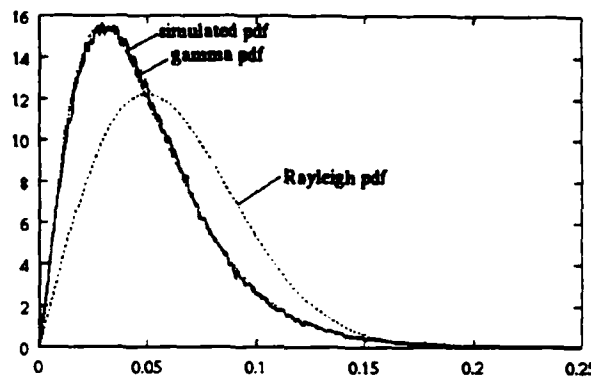**Fig. 15.** The pdf of FWM interference at IF; '0' transmission.

Fig. 16. The pdf of FWM interference at the envelope detector output; '0' transmission.

Fig. 17 shows the simulated pdf's of the sum of the FWM interference terms at IF when the received channel is transmitting '1'. Similar to the '0' transmission case, the main lobe of the in-phase component is seen to match very well with the Student's t-distribution. The quadrature-phase component is shifted from the origin and distorted from the t-distribution shape due to cross-phase modulation. The corresponding Gaussian pdf is also shown in Fig. 17 for comparison. The tails of the simulated pdf's still drop off slower than the Gaussian pdf.

Fig. 18 shows the simulated pdf of the voltage at the envelope detector output for '1' transmission. The main lobe of the simulated pdf is seen to match the t-distribution in this low power case. If the interference had a Gaussian-like behavior at IF, the voltage at the envelope detector output should have a Rician distribution. The corresponding Rician distribution is also shown in Fig. 4 for comparison. It can be also found by expanding the scale in Fig. 18 that the simulation results have larger tails than the Rician distribution corresponding to the Gaussian

20

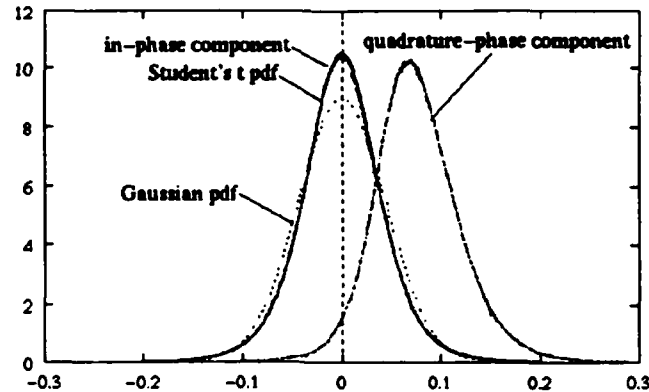approximation. Therefore, the resulting BER is higher in simulation than in Gaussian approximated systems .

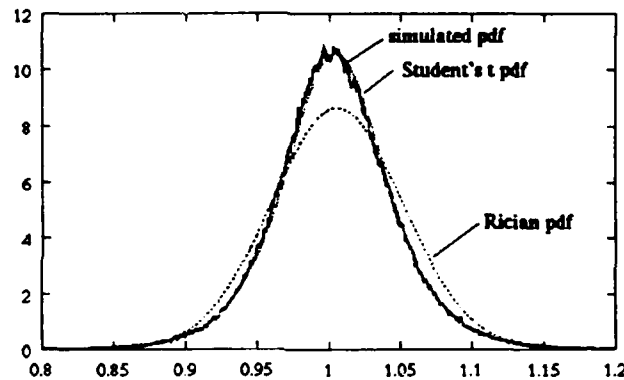**Fig. 17.** The pdf of FWM interference at IF; '1' transmission.

Fig. 18. The pdf of FWM interference at the envelope detector output; '1' transmission.

In summary, the statistical behavior of FWM interference was investigated by computer simulations. The pdf of the FWM interference was found to be non-Gaussian. The distribution at the IF is well approximated by the Student's t-distribution. The resulting pdf at the envelope detector output is well approximated by the gamma distribution and Student's t-distribution for '0' and '1' transmission respectively. The simulated pdf has slower dropping tails than Gaussian pdf.

Impact of Four Wave Mixing on Optical FSK WDM Communication Systems employing Single Filter Envelope Detection Receiver

We theoretically analyze the impact of FWM in a 16 channel optical FSK (frequency-shift-keying) WDM system employing SFED (single-filter-envelope-detection). The analysis takes into account the effects of bandpass filter (BPF) at intermediate frequency (IF) on the FWM

21

interference process. The photodetected IF signal is demodulated by using a BPF at the IF corresponding to the 'mark' transmission followed by an envelope detector and a decision circuit. The BPF input for a receiver tuned to the j-th wavelength can be expressed as

$$i(t) = I_j \cos(\omega_{jM} t + \varphi_j) + \sum_{m=k+l-j} Z_{klm} g_{klm}(t) \cos(\omega_{jM} t + \varphi_{klm}) + n(t) \qquad (3)$$

where, I_j and ϕ_j are the amplitude and phase of the signal component, ω_{jM} is the IF frequency for the mark transmission in the j-th channel, $Z_{klm}(t)$ and ϕ_{klm} represent the amplitude and phase of the FWM interference term produced by k-, l- and m-th channel signals, $g_{klm}(t)$ is a unit amplitude random rectangular pulse train representing the normalized envelope of the same FWM term and, n(t) is the shot noise prior to IF filtering. We consider that the BPF is a bandpass matched filter at ω_{jM}. Since the lowpass equivalent of the BPF is an integrate-and-dump filter, at the end of each bit interval (T) in the desired channel, $g_{klm}(t)$ will result a filtered envelope which can be modeled as a random variable uniformly distributed in [0,T].

Using Eq.(1) we first develop a statistical model for the filtered IF envelope resulting from the interference between the desired signal and the FWM components. At the end of a given interval (consider the 0-th interval in [0,T]), the mark and space envelopes at the BPF output ($a_M(T)$ and $a_S(T)$ respectively) due to the signal-FWM interference can be expressed as

$$a_{M,S}^2(T) = [A_{M,S} + \sum_{klm} B_{klm} \cos(\varphi_{klm} - \varphi_j)]^2 + [\sum_{klm} B_{klm} \sin(\varphi_{klm} - \varphi_j)]^2 \qquad (4)$$

where, A_M and A_S are the filtered signal amplitudes for mark and space ($A_S = 0$) and, B_{klm}'s represent the filtered FWM amplitudes at $t = T$. It is interesting to note that $a_{M,S}(T)$ resemble the carrier envelopes encountered in radio communication channels with multipath fading. Following the similar steps and considering the contribution of filtered $g_{klm}(t)$ in A_M and B_{klm}, the statistics of $a_S(T)$ and $a_M(T)$ are found to follow Rayleigh and Rician distributions respectively. Next we find out the receiver bit error rate (BER) in presence of shot noise with the BER being conditioned on FWM impaired IF envelope following the above statistics. The overall BER is evaluated by averaging the conditional BER over the IF envelope statistics.

The receiver performance is evaluated from the plots of BER in the 8th channel (worst case) versus input optical power in the fiber for different lengths of fibers (effective core area = $55 \mu m^2$, nonlinear susceptibility = $6 \times 10^{-15} cm^3/erg$) with 10 GHz channel spacing and 1Gbps bit rate/channel. Each BER curve exhibits a minimum at a certain power level. This minimum value of BER increases with increase in fiber length and should remain below 10^{-9}. Fig. 19 and 20 show the BER of SFED receivers in 16-channel FSK WDM systems using NDS (non-dispersion-

22

shifted) and DS (dispersion-shifted) fibers, respectively. The dispersion coefficients are 17 ps/nm-km and 0.5 ps/nm-km for NDS and DS fibers, respectively. The maximum transmission distances are 223 km and 195 km for systems using NDS and DS fibers, respectively.
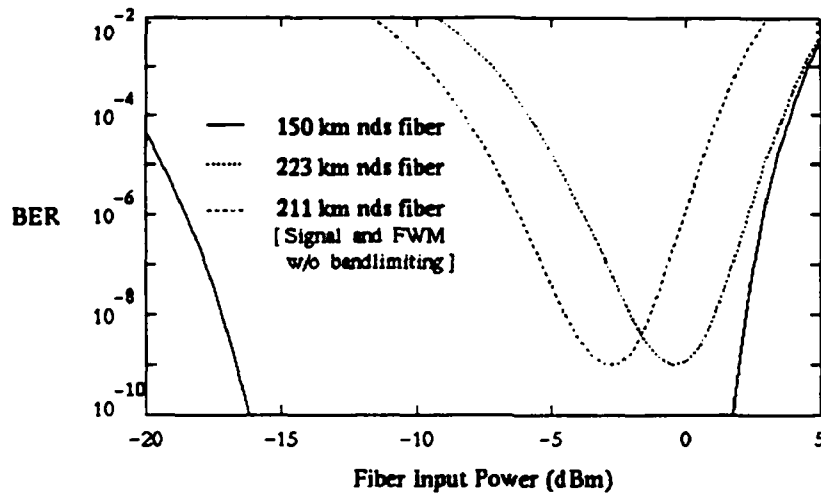
Fig. 19. BER versus fiber input power for SFED receivers in 16-channel FSK WDM systems using NDS (non-dispersion-shifted) fibers.
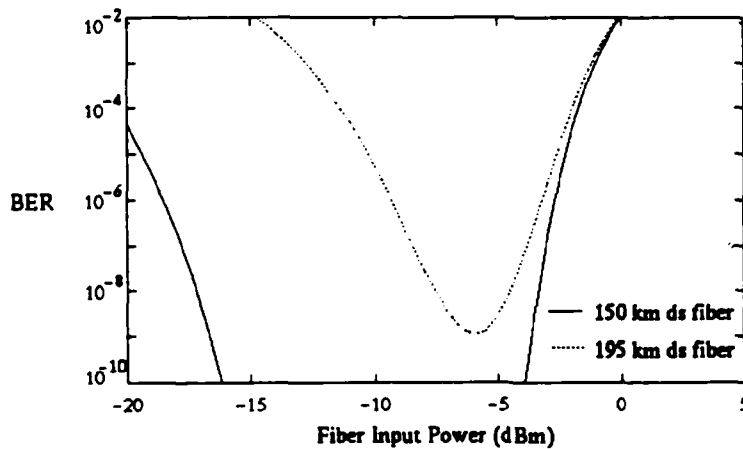
Fig. 20. BER versus fiber input power for SFED receivers in 16-channel FSK WDM systems using DS (dispersion-shifted) fibers.

23

Conclusion: In this report, we presented the progress of our group in three areas, namely: dynamic WDM networks, high dynamic range coherent optical analog links, and fiber nonlinearities. To summarize, we implemented a prototype high-speed interface board of workstation to connect and control the dynamic WDM network, with a data rate of 728 Mbps. To the best of our knowledge, it is the fastest computer interface which has ever been implemented. We also investigated the ASK/DPSK combined modulation formats, which is more tolerable to laser larger laser linewidth than the present ASK/PSK WDM systems. Therefore, it is possible to use more compact and rugged semiconductor laser in the future dynamic WDM network. In the study of coherent analog links, we show conventional DD link has better performance than preamplified DD link and coherent AM link when the received optical power is large. While preamplified DD link and coherent AM link have similar performance over convention DD link when the received optical power is small. Meanwhile, we showed coherent FM and PM analog system are more susceptible to laser linewidth than AM and DD systems. However, if the laser linewidth is negligible, FM and PM system can provide much better SFDR than AM and DD systems. In the area of fiber nonlinearities, the statistics of four wave mixing are investigated by computer simulation. The pdf at the output of envelope is non-Gaussian, and could be well approximated by the gamma distribution and Student's t-distribution for '0' and '1' transmission respectively. We also analyzed the impact of FWM in optical FSK WDM system. The result shows FWM will restrict the maximum transmission distance of the system.

List of Publication between March 1, 1992 and August 31, 1993

I. Papers in refereed journals:

1. G. Fiksman, R. Gross, J. C. Fan, L. G. Kazovsky, "Performance Optimization of Directly Modulated FM-SCM Systems with Optical Discriminator," *IEEE Photonics Technology Letters*, July 1993, Vol. 5, No. 7, pp.845-848.

2. R. F. Kalman, J. C. Fan, L. G. Kazovsky, "A Novel Analog Optical Link with High Dynamic Range," *IEEE Photonics Technology Letters*, June 1993, Vol.5, No. 6, pp.725-728.

3. L. G. Kazovsky and P. T. Poggiolini, "STARNET: a Multi-Gbit/s Optical LAN Utilizing a Passive WDM Star," *IEEE/OSA J. of Lightwave Technology*, Special Issue on Broadband Optical Networks, Vol. 11, May 1993.

4. T. K. Fong, J. Sabido, L. G. Kazovsky, "Linewidth-Insensitive Coherent Analog Optical Link Using Semiconductor Lasers," *IEEE Photonics Technology Letters*, April 1993, Vol. 5, No. 4, pp.469-471.

5. M. Hickey, C. Barry, C. Noronha, L. G. Kazovsky, "Experimental PSK/ASK Transceiver for the STARNET WDM Computer Communication Network," *IEEE Photonics Technology Letters*, Vol. 5, 1993, accepted for publication.

6. O. K. Tonguz, M. O. Tanrikulu, L. G. Kazovsky, "Impact of Finite Frequency Deviation on the Performance of Dual-Filter Heterodyne FSK Lightwave Systems," *IEEE/OSA J. of Lightwave Technology*, Vol. 11, No. 2, February 1993.

7. M. Hickey, L. G. Kazovsky, "The STARNET Coherent WDM Computer Communications Network: Experimental Transceiver Employing a Novel Modulation Formal," *IEEE/OSA J. of Lightwave Technology*, submitted for publication.

8. R. F. Kalman, J. C. Fan, L. G. Kazovsky, "Dynamic Range of Coherent Fiber-optic Links," *IEEE/OSA J. of Lightwave Technology*, submitted for publication.

9. T. Fong, D. J. M. Sabido, R. Kalman, L. G. Kazovsky, "Linewidth-Insensitive Coherent AM Optical Links: Design, Performance, and Potential Application,"*IEEE/OSA J. of Lightwave Technology*, submitted for publication.

II. Conference papers:

1. J. C. Fan, R. F. Kalman, L. G. Kazovsky, "A comparison of Three Analog Optical Links for High Dynamic Range Applications," accepted for presentation at Globecom '93, Houston, TX, November 1993.

2. T. K. Fong, M. Tabara, J. Sabido, L. G. Kazovsky, "Coherent Analog Optical Links: Design, Perfromance and Potentail Applications," accepted for presentation at Globecom '93, Houston, TX, November 1993.

3. M. Tabara, J. Sabido, T. K. Fong, C. L. Lu, L. G. Kazovsky, "A Linewidth-insensitive Coherent AM Optical Link: A Comparison of Derect and EXternal Modulation Format," LEOS Annual '93, Optical Communications.

4. M. Tabara, J. Sabido, T. K. Fong, C. L. Lu, L. G. Kazovsky, "Experimental Investigation of a Linewidth-insensitive Coherent AM Optical Link," LEOS Summer Topicals '93, Optical Microwave Interactions.

5. T. K. Chiang, D. Datta, L. G. Kazovsky, "Statistical Distribution of Four-wave Mixing Interference on ASL Optical WDM Systems," LEOS Summer Topicals '93, Impact of Fiber Nonlinearities on Lightwave Systems.

6. D. Datta, T. K. Chiang, L. G. Kazovsky, "Impact of Four WAve Mixing on Optical FSK WDM Communication Systems," LEOS Summer Topicals '93, Impact of Fiber Nonlinearities on Lightwave Systems.

7. N. L. Taranenko, L. G. Kazovsky, Y. N. Taranenko, "Three-Wave Envelope Solitons: Possibility of Controlling the Speed of Light in the Fiber," URSI General Assembly, Kyoto, Japan, August 1993.

8. R. F. Kalman, J. C. Fan, L. G. Kazovsky, "A Novel Phase-Modulated Analog Optical Link," SPIE's International Symposium OE/Fiber's 93, San Diego, CA, July 1993.

9. J. Sabido, M. Tabara, T. K. Fong, C. L. Lu, L. G. Kazovsky, "Theoretical and Exceptional Investigations of the Dynamic Range of High Frequency Coherent AM Optical Links Using Semiconductor Lasers," SPIE's International Symposium OE/Fiber's 93, San Diego, CA, July 1993.

10. L. G. Kazovsky, C. Barry, M. Hickey, C. Noronha, P. T. Poggiolini, "A Multi-Gbit/s Optical LAN Utilizing a Passive WDM Star: Towards an Experimental Prototype," IEEE INFOCOM, San Francisco, CA, March 1993.

11. T. K. Chiang and L. G. Kazovsky, "Scattering from Guided Acoustic Waves in Optical Fiber and It's Influence on DPSK Optical Communication Systems," OFC '93, San Jose, CA, February 1993.

12. G. Fiksman, R. Gross, J. C. Fan, L. G. Kazovsky, "Optimization of Directly Modulated FM-SCM Systems Using an Optical Frequency Discriminator," OFC '93, San Jose, CA, February 1993.

13. M. Hickey, C. Barry, C. Noronha, L. G. Kazovsky, "An Experimental PSK/ASK Transceiver for a Multigigabit WDM LAN," OFC '93, San Jose, CA, February 1993.

14. H. Lee and L. G. Kazovsky, "Supression of Four-Wave Mixing Crosstalk in WDM Systems Using Manchester Coding and DPSK Modulation," OFC '93, San Jose, CA, February 1993.

15. M. Hickey, C. Barry, C. Noronha, L. G. Kazovsky, "The STARNET Coherent Optical WDM Network: Modulation Format and Computer-to-optics Interface," LEOS summer topical'93, Gigabit Networks.